Journal of Power Sources 188 (2009) 220–224

Contents lists available at ScienceDirect

Journal of Power Sources

journal homepage: www.elsevier.com/locate/jpowsour

Short communication

Mechanical properties of micro-tubular solid oxide fuel cell anodes

Brycen R. Roy[a,*], Nigel M. Sammes[a], Toshio Suzuki[b], Yoshihiro Funahashi[c], Masanobu Awano[b]

[a] Department of Metallurgical and Materials Engineering, Colorado School of Mines, 1500 Illinois Street, Golden, CO 80401, USA
[b] National Institute of Advanced Industrial Science and Technology (AIST), 2266-98 Anagahora, Shimo-Shidami, Moriyama-ku, Nagoya 463-8560, Japan
[c] Fine Ceramics Research Association (FCRA), 2266-98 Anagahora, Shimo-Shidami, Moriyama-ku, Nagoya 463-8560, Japan

ARTICLE INFO

Article history:
Received 28 October 2008
Received in revised form
20 November 2008
Accepted 21 November 2008
Available online 28 November 2008

Keywords:
Strength
SOFC
Anode-support
Micro-tubular
Ceria
Burst test

ABSTRACT

A fundamental issue with micro-tubular solid oxide fuel cells (SOFCs) is improvement of the mechanical strength of the cell. Fabricated using extrusion and co-firing techniques, the approximately 1.7 mm diameter SOFC tubes examined in this work are composed of a 50:50 NiO and $Gd_{0.2}Ce_{0.8}O_{2-x}$ Gd-doped ceria (GDC) cermet anode (support tube), GDC as an electrolyte and $La_{0.8}Sr_{0.2}Co_{0.6}Fe_{0.4}O_3$ (LSCF)–GDC as a cathode. The mechanical properties of SOFCs are analyzed through internal burst testing and micro- and nano-indentation testing; the burst test is an especially important parameter because of improved power efficiency at increased fuel pressures. Results from micro- and nano-indentation tests performed on electrolyte-coated Ni–GDC anode pellets indicate that the hardness of GDC is comparable or greater than that of YSZ. In order to develop a trend for the mechanical behavior of micro-tubes in relation to variations in fabrication techniques, several parameters were varied. The standard anodes, used as a baseline, have four key design parameters as follows: they are not reduced, contain 40 vol% pore former, are sintered at 1400 °C and have a wall thickness of approximately 315 μm. An independent variation on each of the four parameters is performed. The four variations are (1) to reduce the standard tube, (2) to increase the percent pore former to 50% then to 60%, (3) to decrease sintering temperature to 1350 °C, and (4) to decrease the wall thickness to approximately 230 μm. An average burst strength of 22.4 ± 1.5 MPa is observed for the standard tubes, 34.2 ± 16.5 MPa for the reduced tubes, 16.5 ± 4.2 MPa for 50 vol% pore former and 11.7 ± 7.5 for 60 vol% pore former, 29.3 ± 9.6 MPa for the decreased sintering temperature and 34.3 ± 6.9 MPa for the thinner-walled tubes.

© 2008 Elsevier B.V. All rights reserved.

1. Introduction

Solid oxide fuel cell (SOFC) technology has been considered as an alternative source of energy due to its high electrical conversion efficiency, superior environmental performance and fuel flexibility [1–3]. SOFCs have traditionally required high operating temperatures, typically 800–1000 °C yielding slow start-up/shut-down operation and requiring large-scale stationary systems. However, as fabrication techniques have been developed and advanced to allow smaller diameter tubes to be produced, the electrolyte surface area to volume ratio has continued to be enhanced, leading to an increased power density for these tubes [4,5]. The decrease in tube diameter also allows for reduction in wall thickness without any degradation of a cell's mechanical properties [6]. Owing to its thin wall, the micro-tubular SOFC has extremely high thermal shock resistance and low thermal mass [4,5]. These two characteristics are fundamental in reducing start-up and shut-down times for the SOFC system. Improving the power density at reduced operating temperatures also allows for using cost-effective materials for interconnects and balance of plant [7,8]. Finally, reduction in overall system size allows micro-tubular SOFCs to be targeted toward smaller scale applications such as auxiliary power units and other devices requiring portable power [9–11]. It is important that quality electrical properties be balanced with sound mechanical properties. The mechanical strength of fuel cell elements is critically important for a number of reasons. The elements must be able to be handled without breakage during fabrication and stack assembly, and must also survive during the thermal cycling which occurs during normal operation. In these anode-supported micro-tubes, NiO–Gd-doped ceria (GDC) is the anode; the NiO–GDC must be of sufficient thickness and mechanical integrity to provide structural support. Traditional techniques for determining mechanical strength such as 3- or 4-point bending would simply crush the tube walls. A more reliable method for establishing the strength of small thin-walled tubes is to pressurize the inside volume and obtain the strength value at which the tube bursts under the internal pressure. Results from micro- and non-indentation tests performed on electrolyte-coated Ni–GDC anode pellets indicate that the hardness of GDC is comparable or greater than that of YSZ. Values for mechanical tests for GDC can be found in the literature [12,13]. In

* Corresponding author. Tel.: +1 303 273 3640; fax: +1 303 273 3057.
E-mail address: broy@mines.edu (B.R. Roy).

0378-7753/$ – see front matter © 2008 Elsevier B.V. All rights reserved.
doi:10.1016/j.jpowsour.2008.11.076

this study, results for mechanical tests of NiO–GDC anode microtubes are shown, and relationships between fabrication parameters and mechanical properties are discussed.

2. Experimental

2.1. Fabrication

Fabrication of the anode supports follows a similar procedure for fabrication of full cells as developed in a previous study [14]. A plastic mass was created by mixing 0.8 μm NiO powder (Sumitomo Chemical Co., Ltd.), 1 μm $Gd_{0.2}Ce_{0.8}O_{2-x}$ (GDC) powder (Shin-Etsu Chemical Co., Ltd.), 5 μm polymethylmethacrylate (PMMA) beads as the pore former (Sekisui Plastics Co., Ltd.), and cellulose as a binder (Yuken Kogyo Co., Ltd.). Distilled water was added until an extrudable consistency of dough was obtained [15]. The ingredients were mixed together in a vacuum chamber and allowed to age overnight under refrigerated conditions of 36–38 °F (2.2–3.3 °C). The plastic mass was kept in a sealed container during the aging process to avoid over-drying. The dough was then extruded through a metal die forming a 2.3-mm outside diameter and 1.8-mm inside diameter utilizing a piston extruder from ECT. The as-extruded tubes were then dried at room temperature and finally sintered in air by increasing the temperature at 3 °C min^{-1} to either 1350 °C or 1400 °C, holding there for 2 h, and then decreasing the temperature at 3 °C min^{-1} back down to ambient temperature. The sintering temperature was varied for the purposes of this study.

2.2. Burst test apparatus

Average burst-test strengths of the small NiO–GDC anode tubes were determined at room temperature using a custom-built burst-test instrument, shown in Figs. 1 and 2. The pressurized burst test instrument consisted of three components inline: a 10-4000W080 140:1 ratio hydrostatic pump from SC Hydraulic, a Measurement Specialties MSP 5100 Series pressure transducer and a water-tight containment vessel where the actual bursting takes place. All water flow components were Swagelok® medium-pressure fittings, with 1/4″ stainless steel tubing with a wall thickness of 0.065″ up to the ceramic burst sample and flexible high pressure thermoplastic tubing after the ceramic tube. The hydrostatic pump pressurizes water using conditioned compressed air; this air was prepared utilizing a 1.5-hp Husky air compressor and a Wilkerson filter/regulator/lubricator unit to condition the air. Data was collected from the pressure transducer employing a LabJack U3 data acquisition device interfaced through a PC. The setup is capable of pressurizing water up to 34.5 MPa (5000 psi) to fracture the tubes. Tubes of approximately 30 mm in length were adhered to the two stainless steel reducers using various adhesives and bonding materials (30 s set 2-part epoxy, e6000, Corian® glue, un-sintered Ceramabond 552, sintered Ceramabond 552, and combinations of the aforementioned adhesives). The adhesive was required to bond well to both ceramics and metals, dry quickly and withstand pressures potentially at or exceeding 34.5 MPa (5000 psi). Sintered Ceramabond 552, an alumina-based adhesive available from Aremco Products, Inc., outperformed any other adhesive evaluated using the previous defining characteristics. The Ceramabond 552 was applied thoroughly to the outside of the ceramic sample and the stainless tube, allowed to dry at room temperature for approximately 30 min, sintered at 100 °C for 1 h and finally allowed to cool to room temperature before the burst strength was tested. To maintain rigidity of the ceramic micro-tube, an aluminum clamp was designed which would secure the two reducers together, alleviating stresses on the attached burst sample. This clamp, shown in Fig. 3 ensured that the reducers and adhered ceramic tube would move as a "unit" thereby negating breakage from small torques experienced by the tubes while fixing the reducers to the rest of

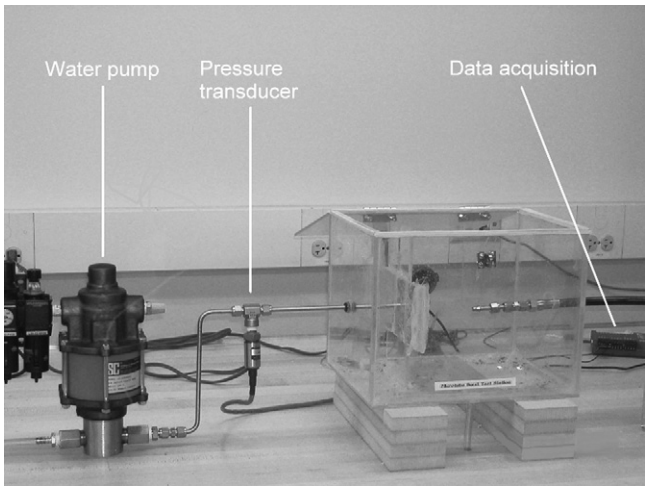

Fig. 1. Burst strength testing apparatus showing the water pump, pressure transducer, and data acquisition device.

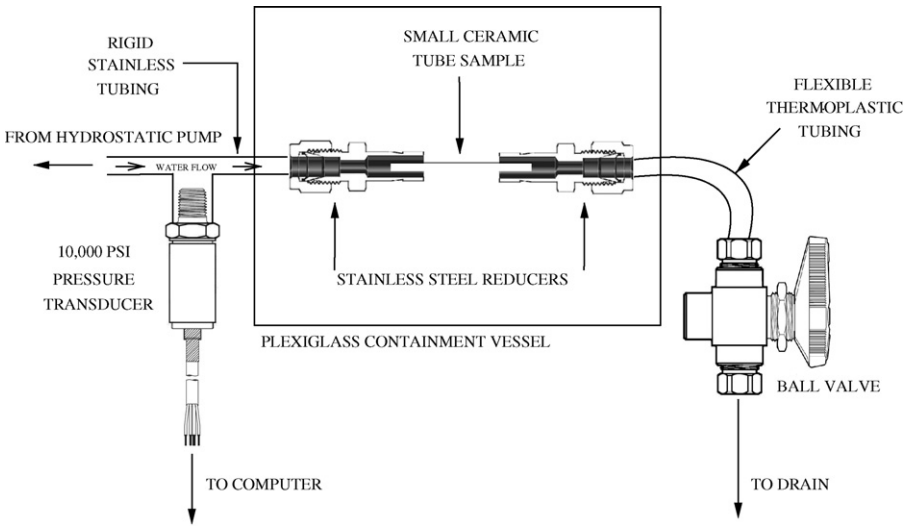

Fig. 2. Schematic representation of the burst testing apparatus.

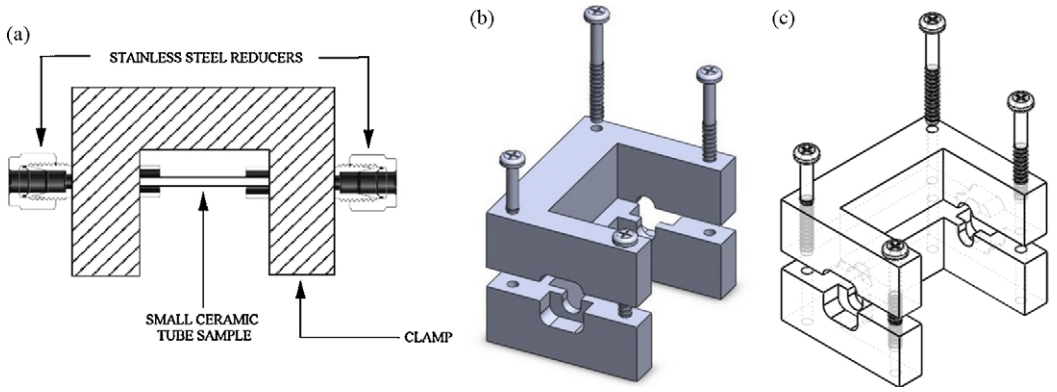

Fig. 3. (a) Schematic representation of the clamp holding a micro-tube bonded to a pair of reducers; (b) isometric solid view of the clamp and (c) trimetric transparent view of the clamp.

the apparatus. Ceramabond 552 was applied with the reducers held firmly in the aluminum clamp. After collecting data, mechanical strengths were calculated from the pressure values at fracture and the dimensions of the tubes. An average of at least 10 values was determined for each tube type.

2.3. Fabrication variations

To develop a trend for the mechanical behavior of micro-tubes in relation to variations in fabrication, several parameters were varied. The standard tubes, used as a baseline for variations, had four key design parameters as follows: they were not reduced, contained 40% pore former by volume, were sintered at 1400 °C and had a wall thickness of approximately 315 μm. Each of these parameters was then varied independently of the other parameters. The first variation was to reduce the standard tube; the second variation was an increase in the percent pore former to 50 vol% and then 60 vol%; the next variation was a decrease in the sintering temperature to 1350 °C for 2 h; the final variation in baseline parameters was a reduction in the wall thickness to approximately 230 μm. The tube reduction was performed by heating the tubes in a hydrogen environment at 5 °C min^{-1} to 600 °C, holding at 600 °C for 1 h, and then letting the tubes cool at 5 °C min^{-1} back down to ambient temperature.

3. Results and discussion

3.1. Hoop stress

Utilizing the custom-built burst test system, burst tests were carried out at room temperature to determine the strength of NiO–GDC tubes. By measuring the burst pressure, the maximum pressure to withstand the gas pressure in a real fuel cell system was determined. Using the assumption that failure was most likely to occur in the radial direction, this maximum pressure was evaluated as a hoop stress. The hoop stress to failure was determined using the equation $\sigma = PD/2t$ where σ is the hoop stress, P is the burst water pressure, D is the inside diameter of the tubes and t is the tube wall thickness. A summary of the calculated hoop stresses is shown in Table 1, and the corresponding Weibull plots are shown in Fig. 4. Also included in the table is a summary of the Weibull statistical analyses performed on the data in the form of Weibull moduli and $\sigma_{0.5}$ values. The $\sigma_{0.5}$ values are a representation of the statistical probability of failure; according to the data 63.2% of the tubes will fail at or before the $\sigma_{0.5}$ value. The Weibull moduli are low for all the tube fabrication variations except the standard tubes. Because one data set is consistent (that is, has a high Weibull modulus), there does not appear to be inconsistency in the experimental process. The large amount of scattering is postulated as being due to a lack of uniformity in the fabrication process. Average hoop stress values can be read directly from the data, and validity of the data can be determined from the Weibull analysis.

3.2. Reduced

There was a particularly large increase in strength of the reduced tubes as compared to the standard tubes, an increase from 22.4 ± 1.5 MPa for the standard tubes to 34.2 ± 16.5 MPa for the reduced tubes. The reduced tubes also show the largest amount of scatter, which could be postulated as being due to variability in the reduction stage. However, all reduced samples still had hoop stress values higher than for the unreduced samples. High strength in reduced tubes is a positive indication for the fabrication of robust stacks.

3.3. Sintering temperature

The next fabrication variation to be discussed is a decrease in sintering temperature from 1400 °C to 1350 °C. Burst strength measurements for the decreased sintering temperature were 29.3 ± 9.6 MPa as compared to 22.4 ± 1.5 MPa for the standard tubes. According to the literature, an increase in sintering temperature causes pores to shrink thereby decreasing the total porosity of the sample; a sintering temperature 1350 °C would have an approximate 5% increase in porosity [10]. Following from the results from variations in pore former addition as discussed in Section 3.5, the

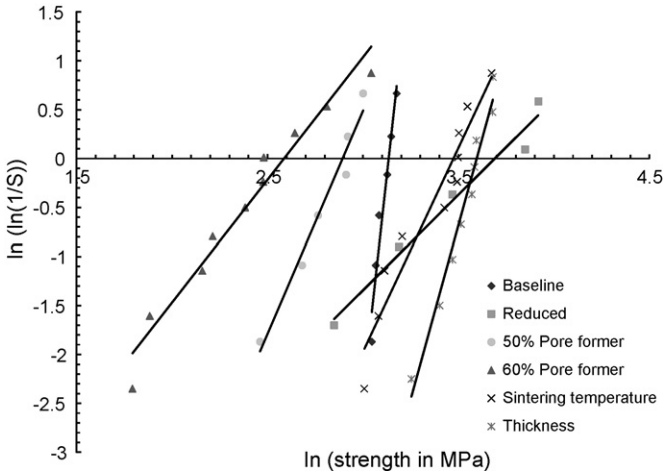

Fig. 4. Weibull plot of hoop stresses from burst tested NiO–GDC anodes.

Table 1
Average hoop stress values calculated from maximum burst strengths for multiple fabrication variations of Ni–GDC anodes.

Sample tube type	Hoop stress (MPa)	Mean strength (MPa) & modulus from Weibull analysis
Ni–GDC, not reduced, 40% pore former, 1400 °C sintering temperature, 315 μm wall thickness	22.4 ± 1.5	$\sigma_{0.5}$ = 23.0, m = 17.8
Ni–GDC, reduced, 40% pore former, 1400 °C sintering temperature, 315 μm wall thickness	34.2 ± 16.5	$\sigma_{0.5}$ = 40.1, m = 1.9
Ni–GDC, not reduced, 50% pore former, 16.5 ± 4.2 1400 °C sintering temperature, 315 μm wall thickness	16.5 ± 4.2	$\sigma_{0.5}$ = 18.0, m = 1.9
Ni–GDC, not reduced, 60% pore former, 11.7 ± 7.5 1400 °C sintering temperature, 315 μm wall thickness	11.7 ± 7.5	$\sigma_{0.5}$ = 13.3, m = 2.5
Ni–GDC, not reduced, 40% pore former, 1350 °C sintering temperature, 315 μm wall thickness	29.3 ± 9.6	$\sigma_{0.5}$ = 32.2, m = 4.2
Ni–GDC, not reduced, 40% pore former, 1350 °C sintering temperature, 230 μm wall thickness	34.3 ± 6.9	$\sigma_{0.5}$ = 36.4, m = 7.1

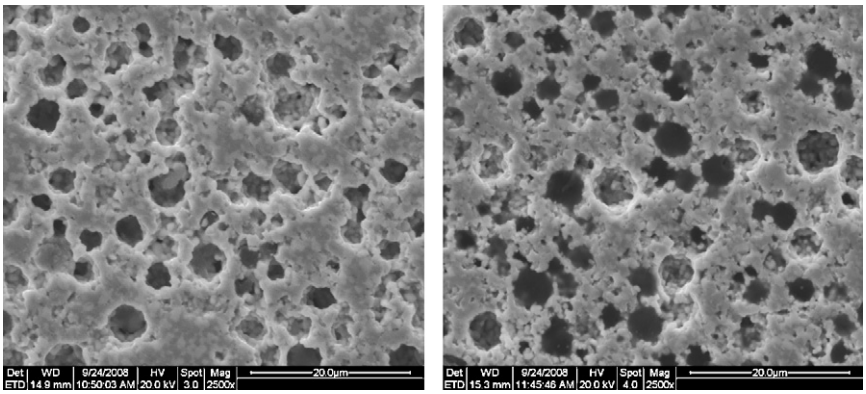

Fig. 5. Cross-sectional SEM images showing small differences in porosity of a NiO–GDC anode at the sintering temperatures of 1400 °C (left) and 1350 °C (right).

porosity increase caused from a lower sintering temperature should lead to a decrease in strength of 10–15%; this outcome was not observed in the tested tubes. Samples were prepared for SEM imaging for both the standard tubes and the tubes with reduced sintering temperatures; representative SEM images are shown in Fig. 5. An original edge detection algorithm was executed on standard SEM images at various locations within the two samples to determine pore boundaries; by this process it was determined that the porosity difference was minimal. Actual porosities of 41% for the standard tube and 43% for the tubes with reduced sintering temperature were observed. The fact that the porosity increased further indicates that previous observations in the literature is correct, but does not explain the increase in strength for tubes with decreased sintering temperature. Multiple backscatter SEM (BSEM) images were taken at the same locations as the standard SEM images. The areas representing open pores were then subtracted from the BSEM images, and percent phase detection (NiO and GDC) was performed on the remainder of the image utilizing a quantitative Otsu multilevel thresholding technique [16]. Visually observing the BSEM images as shown in Fig. 6 and assuming that percent area in the two-dimensional images correlates proportionally to percent volume in the bulk material, it is obvious that there is a large difference in the percent phase between the two sintering temperature samples. The phase percentages determined by the Otsu method were found to be 58% NiO and 42% GDC for the standard tubes and 64% NiO and 36% GDC for the tubes with reduced sintering temperature. The large variation in percent phase between the two samples would explain the apparent difference in strength.

3.4. Wall thickness

Another result was the increased burst strength of tubes with smaller wall thickness as compared to the standard tubes. A reduction in the wall thickness from 315 μm to 230 μm led to an increase in hoop stress from 22.4 ± 1.5 MPa to 34.3 ± 6.9 MPa. Leaving the outside diameter unchanged, a decrease in wall thickness leads to an increase in inside diameter. In relation to the equation for hoop stress, $\sigma = PD/2t$, the direction and amplitude of change for σ is dependent on the tube geometry or $D/2t$. This geometric constant was determined to be 1.947 for the standard tubes and 2.946 for the thinner walled tubes. It would be predicted on a strictly geometrical basis that reducing the wall thickness from

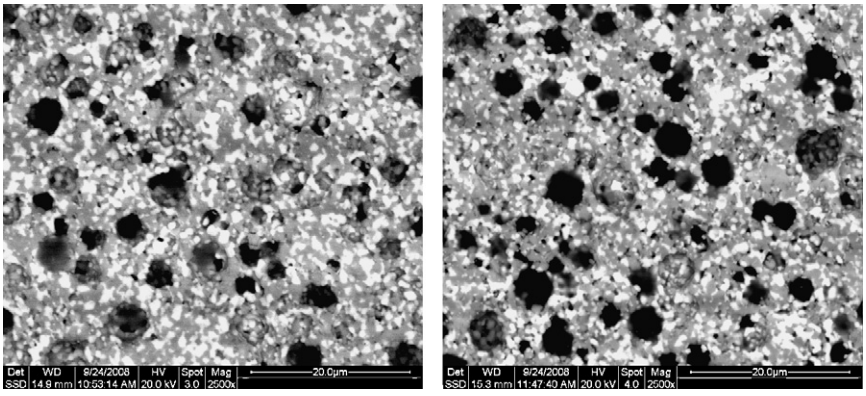

Fig. 6. Cross-sectional backscatter SEM images showing large differences in percent phase NiO and GDC at the sintering temperatures of 1400 °C (left) and 1350 °C (right).

315 μm to 230 μm would lead to an increase in hoop stress of 2.946/1.947 = 1.513 or an approximate 151% increase. The actual increase was (34.3/22.4) × 100% = 153%. This is certainly within experimental limits, but the porosities and percent phase were also found to determine whether the strength increase was solely a function of the reduction in wall thickness. Utilizing the same porosity and percent phase detection algorithm from the sintering temperature variation, the porosity was determined to be 41% (similar to the standard tube) and the phase percentages were determined to be 62% NiO and 38% GDC (as compared to 58% NiO and 42% GDC in the standard tube). The extra 4% NiO in the thinner walled tubes would lead to a greater hoop stress than geometrically predicted, but more data would be needed to determine the absolute increase due exclusively to variations in the anode mixture.

3.5. Porosity

Variations in pore former also had dramatic affects on the burst strength. The increase in porosity generated significant weakness in the tubes as observed by the decrease in burst strengths. There was a linear relationship between percent burst strength decrease and percent increase in vol% pore former. That is, a 25% increase in pore former, from 40 vol% in the standard tubes to 50 vol%, decreased the strength from 22.4 ± 1.5 MPa in the standard tubes to 16.5 ± 4.2 MPa, which is an approximately 26% decrease as compared to the standard tubes. An increase to 60 vol% decreased the strength by 48%, from the aforementioned 22.4 ± 1.5 MPa in the standard tubes to 11.7 ± 7.5 MPa. Utilizing the edge detection and thresholding algorithms discussed previously, the actual porosity of the 50 vol% and 60 vol% anodes was determined to be 51% and 59%, respectively. Phase percentages for the anodes were found to be 55% NiO and 45% GDC for the 50 vol% anode tubes and 57% NiO and 43% GDC for the 60 vol% anode tubes.

4. Conclusions

Anode support-tubes were fabricated using the following parameters for a baseline: they were not reduced, contained 40 vol% pore former, were sintered at 1400 °C and had a wall thickness of approximately 315 μm. A variation on each of the four parameters was performed. The four variations were (1) to reduce the standard tube, (2) to increase the percent pore former to 50 vol% and then to 60 vol%, (3) to decrease sintering temperature to 1350 °C, and (4) to decrease the wall thickness to approximately 230 μm. An average burst strength of 22.4 ± 1.5 MPa was observed for the standard tubes, 34.2 ± 16.5 MPa for the reduced tubes, 16.5 ± 4.2 MPa for 50 vol% pore former and 11.7 ± 7.5 for 60 vol% pore former, 29.3 ± 9.6 MPa for the decreased sintering temperature and 34.3 ± 6.9 MPa for the thinner tubes. From Weibull analysis, moduli of 17.8 MPa, 1.9 MPa, 4.6 MPa, 2.5 MPa, 4.2 MPa and 7.1 MPa were found for the standard, reduced, 50 vol% pore former, 60 vol% pore former, decreased sintering temperature and decreased wall thickness, respectively. The large amount of scattering was most likely due to inconsistencies in fabrication. Even with the poor statistical relevance of the data, it seems evident that reduction of the cell and a decrease in wall thickness lead to an increase in hoop strength, and an increase in porosity yields a decrease in strength. Strength results from a decrease in sintering temperature are inconclusive due to large disparities in fabrication mixtures.

Acknowledgements

This work was supported by the New Energy and Industrial Technology Development Organization (NEDO) under the Advanced Ceramic Reactor Project. The tubes utilized in this study were fabricated by colleagues at AIST and FCRA in Japan.

References

[1] Y. Funahashi, T. Shimamori, T. Suzuki, Y. Fujishiro, M. Awano, J. Power Sources 163 (2007) 731–736.
[2] S. Livermore, J. Cotton, R. Ormerod, J. Power Sources 86 (2000) 411–416.
[3] M. Masashi, H. Yoshiko, N.M. Sammes, Solid State Ionics 135 (2000) 743–748.
[4] N.M. Sammes (Ed.), Fuel Cell Technology: Reaching Towards Commercialization, Springer, Germany, 2006.
[5] J. Pusz, A. Mohammadi, N.M. Sammes, J. Fuel Cell Sci. Technol. 3 (2006) 482–486.
[6] P. Sarkar, Y. Luis, R. Hongsang, J. Lorne, Int. J. Appl. Ceram. Technol. 4 (2007) 103–108.
[7] X. Zhou, J. Ma, F. Deng, G. Meng, X. Liu, J. Power Sources 162 (2006) 279–285.
[8] J. Turner, M.C. Williams, K. Rajeshwar, Electrochem. Soc. Interf. 13 (2004) 24–30.
[9] L. Seung-Bok, L. Tak-Hyoung, S. Rak-Hyun, S. Dong-Ryul, D. Sang-Keun, Int. J. Hydrogen Energy 33 (2008) 2330–2336.
[10] T. Suzuki, Y. Funahashi, T. Yamaguchi, Y. Fujishiro, M. Awano, J. Power Sources 183 (2008) 544–550.
[11] T. Suzuki, Y. Funahashi, T. Yamaguchi, Y. Fujishiro, M. Awano, J. Alloy Compd. 451 (2008) 632–635.
[12] M.C. Williams, J.P. Strakey, W.A. Surdoval, L.C. Wilson, Solid State Ionics 177 (2006) 2039–2044.
[13] X. Xue, J. Tang, N.M. Sammes, Y. Du, J. Power Sources 142 (2005) 211–222.
[14] T. Suzuki, T. Yamaguchi, Y. Fujishiro, M. Awano, J. Power Sources 160 (2006) 73–77.
[15] Y. Du, Ph.D. Dissertation, The University of Waikato, Hamilton, 2004.
[16] P.S. Liao, T.S. Chen, P.C. Chung, J. Comput. Inf. Sci. Eng. 17 (2001) 713–727.